Available online at www.sciencedirect.com

SCIENCE DIRECT®

Earth and Planetary Science Letters 236 (2005) 78–95

EPSL

www.elsevier.com/locate/epsl

Core formation and the oxidation state of the Earth

J. Wade*, B.J. Wood

Department of Earth Sciences, University of Bristol, Wills Memorial Building, Queens Road, Bristol, BS8 1RJ, UK

Received 25 February 2005; received in revised form 13 May 2005; accepted 17 May 2005
Available online 1 July 2005
Editor: S. King

Abstract

We performed experiments to separate the effects of temperature, pressure and metal composition on the metal-silicate partitioning of V, Ni, Co, Mn and Si in order to refine the 'deep magma ocean' model of core formation. Interactions in the liquid metal were accounted for by using a well-known metallurgical model combined with data from the literature. Temperature effects were calculated using free energy data for liquid metals and liquid oxides. This approach enabled us to separate pressure effects from those of the other two variables.

If we assume that the core formed by a single-stage process then we find that the mantle concentrations of the refractory elements can be matched at a temperature of 3750 K and a pressure of 40 GPa. These values are in good agreement with recent estimates based on other partitioning data. The calculated temperature is, however, 700 °C above the peridotite liquidus at 40 GPa, and is therefore physically implausible. The base of the magma ocean, at which metal would pond during accretion must be saturated in crystals and should, therefore lie at or below the silicate liquidus. We find that dynamic accretion models, in which pressure increased as the earth grew, do not improve the match to the peridotite liquidus so long as the oxygen fugacity is fixed by the current Fe content of the mantle. If, however, we force temperature to lie on the peridotite liquidus as the earth grew, the mantle concentrations of refractory elements can be matched provided oxygen fugacity increased during accretion. To illustrate this we use accretionary models in which, as the earth grew, the base of the magma ocean was at half the mantle depth and applied gradual or step-changes in oxygen fugacity. If we apply a 2 log unit increase in oxygen fugacity, the siderophile element contents of the mantle are matched, the Si content of the core is 5 to 7 wt.% and the average core segregation temperature is 2990 K, within the experimental range.

Oxidation during accretion is an important component of heterogeneous accretion models, but the mechanisms proposed are generally untestable. Here we propose that an increase in oxidation state is a natural consequence of the size of the earth. Magnesium silicate perovskite is the principal phase in the earth's lower mantle. This phase forces the disproportionation of ferrous iron into ferric iron plus metal. When perovskite started to grow at the base of the magma ocean, dissolution and reprecipitation acted as an 'oxygen pump' injecting oxidized ferric iron into the upper mantle. As the earth continued to grow, infalling metal was oxidized by the ferric iron into ferrous iron, raising the iron content of the magma ocean and the oxygen fugacity of metal-silicate equilibration. This process did not occur to any great extent on Mars because of the limited stability of perovskite in the smaller planet

Keywords: Earth accretion; core formation; metal-silicate partitioning; mantle-oxidation state; perovskite

* Corresponding author.
E-mail addresses: Jon.Wade@bris.ac.uk (J. Wade), b.j.wood@bris.ac.uk (B.J. Wood).

0012-821X/$ - see front matter © 2005 Elsevier B.V. All rights reserved.
doi:10.1016/j.epsl.2005.05.017

1. Introduction

The earliest history of the Earth was marked by accretion and core segregation with a mean Hf–W age of about 11 Ma after the formation of the solar system [1,2] and formation of the moon by giant impact approximately 35 Ma later [3]. Although there is no remaining geological evidence of these profound events, radiogenic isotopes (for example [1,2]) provide information on their timing while dynamical modeling yields insight into the physics of planetary formation [4]. Given that the bulk composition of the Earth has strong affinities with those of chondritic meteorites [5,6], the process of core formation is reflected in the depletions of the primitive mantle, relative to chondrites, in siderophile elements such as Ni, Co and W [5,6].

During segregation of the core all elements were distributed between the Fe-rich metallic phase and the silicate mantle according to their partition coefficients D_i defined as follows:

$$D_i = \frac{[i]_{\text{metal}}}{[i]_{\text{silicate}}} \quad (1)$$

where $[i]$ is the concentration of element I in the phase of interest. Elements with high values of D (siderophile) are strongly depleted in the mantle while those with low D values (lithophile) are present in the mantle in approximately chondritic proportions [5–7]. If we make the simplest assumption, that the core separated from the mantle under equilibrium conditions, then we need to consider D_i values in terms of the redox reaction:

$$\mathrm{MO}_{n/2} = \mathrm{M} + \frac{n}{4}\mathrm{O}_2 \quad (2)$$

Reaction (2) represents reduction of the element as it transfers from its normal oxidation state (n) in the silicate to oxidation state zero in the metal. Given a concentration of FeO in the mantle of about 8 wt.% and of Fe in the core of 80% [5,6], reaction (2) implies that the core separated from the mantle at an oxygen fugacity approximately 2 $\log fO_2$ units below Fe–FeO (IW) equilibrium. Under these oxygen fugacity conditions, measured partition coefficients of Ni and Co at low pressures and temperatures are, respectively, about 50 and 5 times too high to explain the observed concentrations of these elements in the mantle [8]. This has led to the so-called 'excess siderophile problem' reflecting Ni and Co contents of the mantle which are substantially higher than would be anticipated from core–mantle equilibrium.

One possible solution to the 'excess siderophile problem' is provided by the heterogeneous accretion model [9]. This assumes separation of the core under conditions which became more oxidizing with time. Since it is estimated that the surface of the growing planet began to melt when it reached about 20% of its current size [10], it is likely that a substantial proportion of the core equilibrated with the mantle under relatively low pressure conditions. The only way that this can be consistent with the low pressure partitioning data is if the oxygen fugacity of equilibrium increased such that all elements became less siderophile towards the end of accretion. The final step in the heterogeneous accretion model is the addition of the highly siderophile elements (Pt, Au, Re, Os, etc.) to the silicate mantle as a 'late veneer' after core formation ceased [5,11,12].

An alternative approach to the excess siderophile problem is based on the increasing number of high pressure partitioning data which have recently become available. These data show that the partition coefficients of some siderophile elements (most notably Ni and Co) decrease with increasing pressure [13,14] such that their mantle abundances may be explained by metal-silicate equilibrium at average conditions of around 28 GPa and 2000 °C [13]. These observations led to the 'deep magma ocean' hypothesis which, at its simplest, is interpreted as core–mantle equilibration at fixed pressure, temperature and oxygen fugacity. In this interpretation (e.g. [13] [15]), droplets of metallic liquid descended through a 700 km deep (28 GPa) magma ocean, equilibrating with the silicate liquid as they fell [16]. The liquid metal ponded at the base of the magma ocean and subsequently descended in large diapirs to the growing core without further equilibration with the surrounding silicate (Fig. 1). The principal objection to this model is that it is unlikely that one set of P–T conditions can satisfy the mantle abundances of all elements. Also, as generally recognized, the 'unique' equilibration conditions more plausibly represent an average of a wide range of conditions generated during an extremely dynamic process. Nevertheless, the 'deep

magma ocean model' does have the important property of a scientific hypothesis, that it is amenable to experimental testing.

Experiments performed in the diamond-anvil cell [17] appear to support the suggestion that the siderophile character of Ni and Co decreases with increasing pressure. In the latter case, however, a much higher pressure of core–mantle equilibrium, 45 GPa equivalent to at least 1200-km depth in the present-day Earth was obtained. There is also, potentially, a strong temperature effect on metal-silicate partitioning, as was pointed out by Rama Murthy [18]. Since the melting temperatures of both silicates and metals increase with pressure, increasing experimental pressure tends to be accompanied by increasing temperature. This makes it extremely difficult to separate the effects of the two variables and means that some of the observed 'pressure effect' may actually be due to increasing temperature. Additional experimental uncertainties arise from the use, in some studies, of graphite capsules which contaminate the metal with substantial amounts of carbon and the employment of iron sulphide instead of iron metal in other studies. Both of the non-metals, carbon and sulphur can, as is well-known in the metallurgical literature (e.g. [19]), strongly influence the thermodynamic properties of trace substituents and hence change partitioning behaviour.

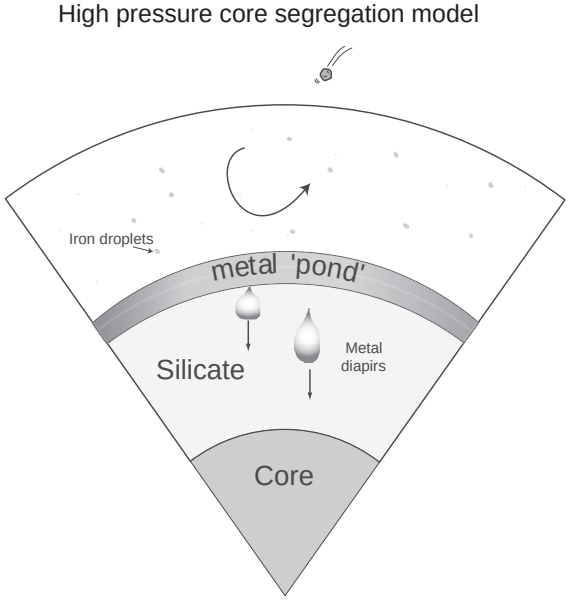

Fig. 1. Model of core segregation at the base of a deep magma ocean. Droplets of metallic liquid descend through the magma ocean, equilibrating with the surrounding silicate melt. The metal ponds at the base of the silicate layer. It then forms large diapirs which descend rapidly to the growing core without further equilibration with the surrounding silicate. This simple model generates partitioning behaviour consistent with observed mantle abundances of Ni and Co (after [12],[14] and [15]).

Given the importance of the high pressure partitioning data for testing models of core formation our goals, in this study, were to extend and refine the database by:

(a) Separating the effects of temperature from those of pressure on the metal-silicate partitioning of Ni, Co, V, Si and Mn. To this end we have performed isobaric partitioning experiments over a temperature range of greater than 800 °C and have used end-member thermodynamic data as constraints on the temperature-dependencies of partition coefficients.
(b) Correcting partition coefficient data for the known influences of other elements such as C, Si and S in the metal in order to minimize matrix effects on the experimental results. This has been done using thermodynamic data from the literature.

The final section of the paper deals with the application of our new results, together with data in the literature, to estimation of the conditions of core formation. As will be shown, the data are most consistent with metal-silicate equilibration at the base of a magma ocean which deepened during accretion and in which the oxygen fugacity increased with time. This 'best' solution thus contains the most important elements of both the heterogeneous and homogeneous (magma ocean) models.

2. Experimental methods

We performed liquid metal-liquid silicate partitioning experiments at low (2.0 GPa) and high (25 GPa) pressures for a range of siderophile trace elements under conditions where the metal contains between <0.02% and 11.6% Si. Although Ni and Co-bearing experiments had Si-free metal, addition of Si enabled us to reduce oxygen fugacity to the conditions under

which Mn became siderophile, even at low temperature. Experimental starting materials were equal proportions of natural $Forsterite_{90}$ and a metallic component containing appropriate proportions of Fe and $Fe_{83}Si_{17}$. Experiment R3 used a synthetic basalt reduced at 1000 °C in a CO/CO_2 atmosphere at 2 $\log f O_2$ units below the fayalite–magnetite–quartz buffer, as the silicate component. Starting materials were intimately ground under acetone together with a trace element component consisting of oxides of Fe, Mn, Cr, V, Co and Ni. All 2.0 GPa experiments were performed in carbon capsules, using high temperature piston cylinder assemblies [20]. At 2173 K experiments were held at temperature for approximately 20 min, while 3000 K experiments were held at temperature for approximately 90 s. The 25-GPa experiments were performed using the multi-anvil apparatus at the Bayerisches Geoinstitut (Bayreuth) and contained within single crystal MgO capsules. Details of assemblies and pressure calibration may be found in [21,22]. Samples were held at 3000 K for approximately 90 s. In all cases, experiment duration was limited by the inviscid nature of the experimental charge, which tends to escape from the capsule at high temperature. Temperature control in all experiments was via a W/Re thermocouple, placed directly above the capsule and the experiment was quenched by turning off the power to the furnace. For the high temperature experiments, the thermocouple failed consistently at ~2900 K, with the final temperature being estimated from extrapolation of the temperature vs power curve. Analysis was performed using the JEOL 8600 electron microprobe at the University of Bristol using a range of metal, oxide and silicate standards and conditions of 20 kV accelerating voltage with 15 nA beam current. All microprobe corrections were made using the phi–rho–z approach and a number of well-known standards such as St. John's Island olivine and KK1 hornblende employed as checks on the calibration. Carbon was not measured by microprobe. Metals contained in carbon capsules routinely quenched to C-bearing alloys containing laths of graphite. Therefore the microprobe totals which, because of the presence of carbon, are less than 100.0, actually indicate lower carbon concentrations than were present during the experiment because some dissolved carbon has precipitated as graphite. Experimental data are presented in Table 1.

3. Interactions of solutes in metal alloys

Experimental data on the partitioning of minor elements between metals and silicates have been collected over wide ranges of conditions of pressure, temperature and composition. In order to achieve a measurable result it is frequently necessary to modify the composition of the alloy such that it bears only passing resemblance to the composition of the core. In some cases, as here, Si is added to reduce the oxygen fugacity; in others the 'trace' elements are added at extremely high concentration levels while frequently there are substantial quantities of S and C present in the alloy. Since all of the elements of interest are known to interact with one another in metallic liquids [23], partitioning experiments performed under different compositional conditions are bound to produce scattered results. In order to correct, as far as possible, for these interactions we employed a thermodynamic approach which has been specifically developed for iron alloys [24].

The 'Wagner ε formalism' [24] represents the effects of different solutes on one another's thermodynamic properties as follows:

$$\ln\gamma_i = \ln\gamma_i^o + \sum_{j=2}^{N} \varepsilon_i^j x_j \qquad (3)$$

In Eq. (3), γ_i is the activity coefficient of solute i in the mixed alloy and γ_i^0 is its activity coefficient when it is infinitely dilute in pure liquid Fe under the same conditions of pressure and temperature. The interaction parameters ε_i^j refer to the measured effects of component j on the activity of i in the alloy and are assumed to be linearly dependent on the mole fraction of j, x_j. A large number of experiments have been interpreted in terms of this formalism and the results tabulated in publications such as the Steelmaking Data Sourcebook [23]. Unfortunately, however, the Wagner formalism is only thermodynamically consistent at very high dilution, so modifications need to be made for alloys, as frequently employed in high pressure experiments, where concentrations of solutes are high. One approach, the 'unified ε formalism' [25] employs a thermodynamically consistent model which is similar to Eq. (3) but in which

Table 1

	HT FeC	2σ	HT60	2σ	HT8020c	2σ	HT70	2σ	HT30	2σ	HT40	2σ	LT11	2σ	LT21	2σ	LT20	2σ
Temp (K)	3000		3000		3000		3000		3000		3000		2173		2173		2173	
Pressure (GPa)	2		2		2		2		2		2		2		2		2	
Sillicate																		
O*	44.10		45.29		45.84		46.15		45.94		46.78		44.87		46.03		46.89	
Na																		
Mg	31.16	0.29	30.14	0.45	31.13	0.46	31.45	0.24	35.19	0.38	31.40	0.19	31.91	0.40	30.30	0.08	30.21	0.71
Al																		
Si	18.89	0.23	21.64	0.23	21.47	0.21	22.21	0.18	19.93	0.12	22.84	0.16	19.61	0.19	22.19	0.58	23.60	0.51
Ca																		
Ti																		
V	0.26	0.06	0.09	0.01	0.11	0.01	0.01	0.00					0.16	0.05	0.07	0.01		
Cr	0.19	0.04	0.07	0.01	0.10	0.01							0.10	0.02	0.05	0.01		
Mn	0.63	0.05	0.46	0.03	0.68	0.05	0.19	0.01	0.05	0.01	0.14	0.01	0.47	0.05	0.69	0.08	0.23	0.03
Fe	5.54	0.53	1.91	0.10	1.90	0.11	0.28	0.02	0.21	0.05	0.18	0.02	4.29	0.54	1.60	0.24	0.16	0.03
Co																		
Ni																		
Zr																		
Nb	0.41	0.14	0.14	0.03	0.21	0.05	0.02	0.01					0.09	0.19	0.21	0.06		
W																		
Silicate total	101.17	0.32	99.74	0.43	101.44	0.24	100.30	0.22	101.31	0.70	101.33	0.15	101.50	0.49	101.14	0.48	101.09	0.43
Metal																		
X_C-Calculated*	0.36		0.37		0.37		0.35		0.34		0.29		0.24		0.24		0.20	
Al																		
Si			0.12	0.03	0.06	0.03	2.67	0.29	3.75	0.10	11.62	0.16			0.02	0.01	5.36	0.06
V	0.19	0.03	0.53	0.04	0.78	0.14	0.62	0.07	0.52	0.06	0.60	0.04	0.09	0.01	0.44	0.01	0.42	0.04
Cr	0.46	0.06	0.56	0.02	0.87	0.10	0.62	0.07	0.59	0.06	0.87	0.03	0.31	0.03	0.49	0.01	0.48	0.03
Mn	0.04	0.01	0.24	0.05	0.36	0.08	0.68	0.04	0.48	0.03	1.12	0.04	0.03	0.00	0.15	0.01	0.62	0.02
Fe	90.08	0.58	90.80	0.56	89.89	1.74	88.31	0.53	85.90	1.04	78.90	0.94	89.76	0.26	88.59	0.18	85.57	0.51
Co	0.83	0.02	0.71	0.03	0.81	0.11	0.52	0.05	0.66	0.02	0.92	0.02	0.88	0.02	0.70	0.02	0.61	0.01
Ni	1.24	0.07	1.12	0.05	1.12	0.17	0.80	0.06	0.87	0.03	1.22	0.02	1.26	0.02	1.01	0.03	0.92	0.02
Nb	0.01	0.01	0.55	0.07	0.65	0.17	0.72	0.86	0.70	0.11	0.49	0.06	0.01	0.01	0.46	0.02	0.54	0.07
W	0.99	0.12	1.39	0.14	1.46	0.63	2.23	0.32	1.66	0.23	1.36	0.09	1.25	0.06	1.17	0.08	1.03	0.11
Metal sum	93.84	0.58	96.02	0.39	96.01	1.01	97.17	0.35	95.14	1.05	97.11	1.11	93.59	0.26	93.01	0.21	95.55	0.36

	LT30	2σ	LT40	2σ	s2266	2σ	s2265	2σ	R3	2σ	2000Co	2σ	2700Co	2σ	2000Ni	2σ	2700Ni	2σ
Temp (K)	2173		2173		3000		3000		2473		2273		3000		2273		3000	
Pressure (GPa)	2		2		25		25		2		2		2		2		2	
Silicate																		
O*	47.15		46.18		43.83		43.30		45.35		43.94		44.20		43.42		44.67	
Na									5.20	0.07								
Mg	28.26	1.54	29.31	0.25	23.24	1.46	21.93	1.35	8.30	0.06	31.60	0.29	31.85	0.47	30.78	0.49	33.29	0.24
Al									8.04	0.02								
Si	24.96	1.06	23.50	0.18	21.94	0.94	21.85	0.97	24.12	0.06	18.97	0.12	19.27	0.14	18.98	0.10	19.38	0.11
Ca									5.13	0.02								
Ti									0.77	0.01								
V					0.74	0.09	1.06	0.08	0.11	0.01			1					
Cr	0.02	0.00			0.38	0.06	0.66	0.04	0.12	0.01								
Mn	0.24	0.04	0.28	0.01	1.19	0.12	1.88	0.16	1.11	0.02								
Fe	0.15	0.02	0.11	0.02	5.81	0.35	5.77	0.44	1.41	0.11	4.70	0.35	3.89	0.69	5.20	0.74	2.21	0.34
Co					0.02	0.00	0.02	0.00			0.68	0.03	0.64	0.07				
Ni					0.01	0.00	0.01	0.00							0.17	0.01	0.18	0.01
Zr																		
Nb					2.33	0.75	2.35	0.59	0.11	0.00								
W																		
Silicate total	100.78	0.32	99.38	0.24	99.50	0.41	98.84	0.38	99.78	0.12	99.89	0.33	99.86	0.35	98.54	0.26	99.73	0.25
Metal																		
X_C-Calculated*	0.20		0.18		0.00		0.00		0.28		0.21		0.33		0.19		0.32	
Al																		
Si	5.72	0.06	8.57	0.33	1.60	0.03	0.94	0.05	0.28	0.05								
V	0.39	0.03	0.84	0.05	0.23	0.01	0.24	0.02	0.95	0.05								
Cr	0.47	0.03	1.20	0.06	0.59	0.01	0.63	0.02	1.12	0.03								
Mn	0.63	0.02	1.39	0.05	0.48	0.01	0.47	0.03	0.31	0.06								
Fe	85.02	0.30	80.11	0.29	91.03	0.24	90.78	0.33	85.34	0.47	50.65	1.72	51.13	0.47	48.11	1.20	52.75	0.86
Co	0.62	0.01	1.14	0.03	1.23	0.01	1.39	0.01	1.20	0.04	44.72	1.13	47.84	0.50				
Ni	1.13	0.03	1.58	0.05	1.43	0.01	1.55	0.01	1.58	0.06					48.20	1.91	44.75	0.93
Nb	0.52	0.04	0.62	0.06	0.38	0.07	0.31	0.09	0.90	0.28								
W	1.08	0.08	1.58	0.13	1.81	0.09	2.18	0.10	2.24	0.38								
Metal Sum	95.58	0.22	97.01	0.35	98.77	0.19	98.49	0.21	93.93	0.22	95.37	1.23	98.97	0.07	96.31	0.92	97.49	0.19

[+] Oxygen in silicate calculated by stoichometry.

[0] Metal generally contains carbon which has not been determined by microprobe.

* Mole fraction of carbon in the metallic phase, calculated from the Fe–C system summarised by Wood (1993) [45] with other interactions calculated using ε approach as described in the text.

the interaction parameters are generally slightly different. In order to use the tabulated ε values directly, we opted for the approach of Ma [26] which employs exactly the same parameters, but which is thermodynamically consistent and obeys the Gibbs–Duhem equation. Since most of the interaction parameters and infinite dilution activity coefficients (γ_i^0) were obtained at temperatures close to 1873 K, we extrapolated them to higher temperatures using the approach suggested in the Steelmaking Data Sourcebook:

$$\ln\gamma_i^o(T) = \frac{T^o}{T}\ln\gamma_i^o(T^o)$$

$$\varepsilon_i^j(T) = \frac{T^o}{T}\varepsilon_i^j(T^o) \quad (4)$$

where T is the temperature of interest and T^o is the temperature at which the tabulated values apply.

The 'interaction parameter' approach has been applied as far as possible to available literature data on metal-silicate partitioning. Since, however, this model is based on alloy results obtained at fairly low mole fractions of solutes (generally <0.2) it is not always applicable to high concentrations of strongly-interacting elements such as S, C and Si. For this reason we have excluded data on V and Mn partitioning when the mole fraction of S in the liquid was greater than 0.1, since these two elements interact strongly with S [23]. In order to be able to use the substantial body of data on Ni and Co partitioning with high S-liquids we estimated their activities on the Fe–FeS join from the nonmetal segregation model of Jones and Malvin [27].

4. Calculation of equilibrium constant and partition coefficients

Reaction (1) describes the redox equilibrium governing the partitioning of element M between metal and silicate. Application of this to experimental results requires use of activity coefficients in metal and silicate, as discussed above, and an estimate of oxygen fugacity. The latter, defined in terms of Fe–FeO equilibrium, necessitates knowledge of the mixing properties of FeO in the silicate melt, something which is poorly known. An alternative approach, which we take here, is to consider partitioning as an exchange reaction involving Fe, FeO and the oxidized and reduced components of element M:

$$\mathrm{MO}_{n/2} + \frac{n}{2}\mathrm{Fe} = \frac{n}{2}\mathrm{FeO} + \mathrm{M} \quad (5)$$

silicate metal silicate metal

This is a useful way of avoiding precise definition of oxygen fugacity, but requires knowledge of n, the oxidation state of the trace ion in the silicate melt. Thus it may not be readily applicable to elements such as Cr which have more than one oxidation state in the oxygen fugacity range of interest. The equilibrium constant for reaction (5) is defined in terms of activities of components a_i, their mole fractions x_i and activity coefficients γ_i as follows:

$$K_a = \frac{\left(a_{\mathrm{FeO}}^{\mathrm{Sil}}\right)^{n/2}\cdot\left(a_{\mathrm{M}}^{\mathrm{met}}\right)}{\left(a_{\mathrm{Fe}}^{\mathrm{met}}\right)^{n/2}\cdot\left(a_{\mathrm{MO}_{n/2}}^{\mathrm{Sil}}\right)} = \left[\frac{\left(x_{\mathrm{FeO}}^{\mathrm{Sil}}\right)^{n/2}\cdot\left(x_{\mathrm{M}}^{\mathrm{met}}\right)}{\left(x_{\mathrm{Fe}}^{\mathrm{met}}\right)^{n/2}\cdot\left(x_{\mathrm{MO}_{n/2}}^{\mathrm{Sil}}\right)}\right] \times \frac{\left(\gamma_{\mathrm{FeO}}^{\mathrm{Sil}}\right)^{n/2}\cdot\left(\gamma_{\mathrm{M}}^{\mathrm{met}}\right)}{\left(\gamma_{\mathrm{Fe}}^{\mathrm{met}}\right)^{n/2}\cdot\left(\gamma_{\mathrm{MO}_{n/2}}^{\mathrm{Sil}}\right)} \quad (6)$$

In Eq. (6) the term in square brackets (K_D) is what is measured experimentally, activity coefficients in the metal were obtained as discussed above which leaves those for the silicate as the principal unknowns. Taking logarithms and rearranging yields:

$$\log K_a = \log\left[\frac{\left(x_{\mathrm{FeO}}^{\mathrm{Sil}}\right)^{n/2}\cdot\left(x_{\mathrm{M}}^{\mathrm{met}}\right)}{\left(x_{\mathrm{Fe}}^{\mathrm{met}}\right)^{n/2}\cdot\left(x_{\mathrm{MO}_{n/2}}^{\mathrm{Sil}}\right)}\right] + \log\frac{\left(\gamma_{\mathrm{M}}^{\mathrm{met}}\right)}{\left(\gamma_{\mathrm{Fe}}^{\mathrm{met}}\right)^{n/2}} + \log\frac{\left(\gamma_{\mathrm{FeO}}^{\mathrm{Sil}}\right)^{n/2}}{\left(\gamma_{\mathrm{MO}_{n/2}}^{\mathrm{Sil}}\right)} \quad (7)$$

For each experiment we evaluated the first two terms on the right hand side of Eq. (7) and plotted them as a function of reciprocal temperature as shown in Figs. 2–6. Provided the ratio of oxide activity coefficients is not a strong function of silicate melt composition, the first two terms should

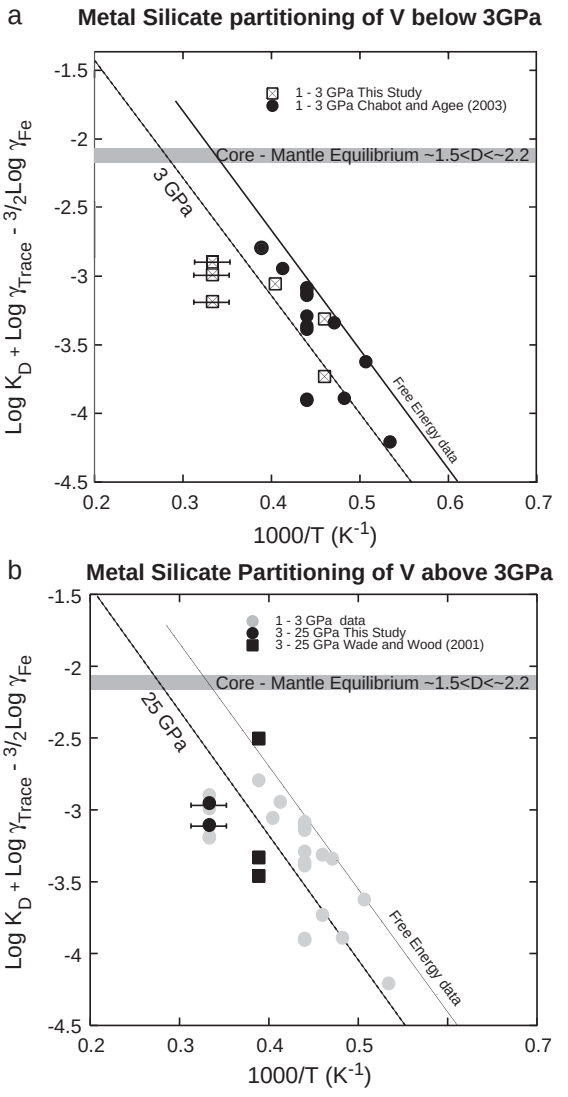

Fig. 2. The modified equilibrium constant for vanadium $\log\left[K_D^{\mathrm{V}}\right] + \log\left(\gamma_{\mathrm{V}}^{\mathrm{met}}\right) - \log\left(\gamma_{\mathrm{Fe}}^{\mathrm{met}}\right)^{3/2}$ plotted as a function of $1000/T$ for experimental data from this and other studies (see text). Solid lines represent 1 bar free energy data taken from [29,30], while dashed lines correspond to the best-fit equation at 3 and 25 GPa (see text). The horizontal dark grey field represents the values of equilibrium constant required to generate the observed mantle abundance of V([5,7]). This corresponds to $D_{\mathrm{V}} = \frac{[\mathrm{V}]_{\mathrm{metal}}}{[\mathrm{V}]_{\mathrm{silicate}}}$ of about 1.5 to 2.2 (see Table 2). Data taken from [31,46].

yield apparent values of log K_a which have the same temperature dependencies as log K_a calculated from end-member free energy data. In defence of this assumption, O'Neill and Eggins [28] show that it applies for FeO/NiO and FeO/CoO over a wide range of compositions. Data collected in our laboratory (M.V. Lee, personal communication) indicate that a similar assumption works well for MnO and

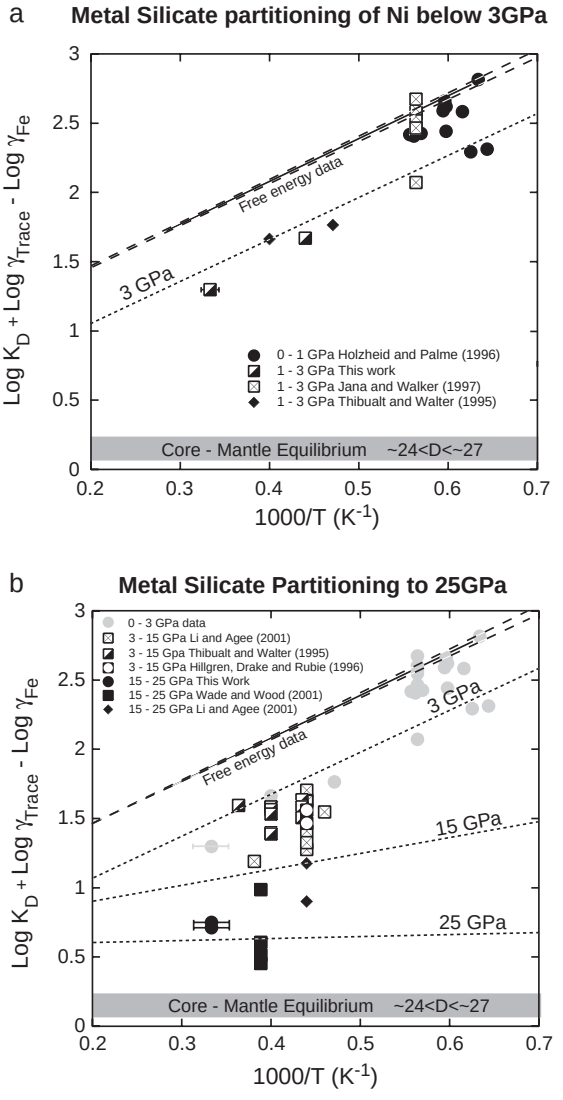

Fig. 3. The modified equilibrium constant for nickel, $\log\left[K_D^{\mathrm{Ni}}\right] + \log\left(\gamma_{\mathrm{Ni}}^{\mathrm{met}}\right) - \log\left(\gamma_{\mathrm{Fe}}^{\mathrm{met}}\right)$ plotted as a function of $1000/T$ for experimental data from this and other studies (see text). Solid lines represent 1 bar free energy data taken from [29,30], while dashed lines correspond to the best-fit equation at 3, 15 and 25 GPa (see text). The horizontal dark grey field represents the values of equilibrium constant required to generate the observed mantle abundance of Ni ([5,7]). This corresponds to $D_{\mathrm{Ni}} = \frac{[\mathrm{Ni}]_{\mathrm{metal}}}{[\mathrm{Ni}]_{\mathrm{silicate}}}$ of about 24 to 27 (Table 2). Data taken from [14,46–50].

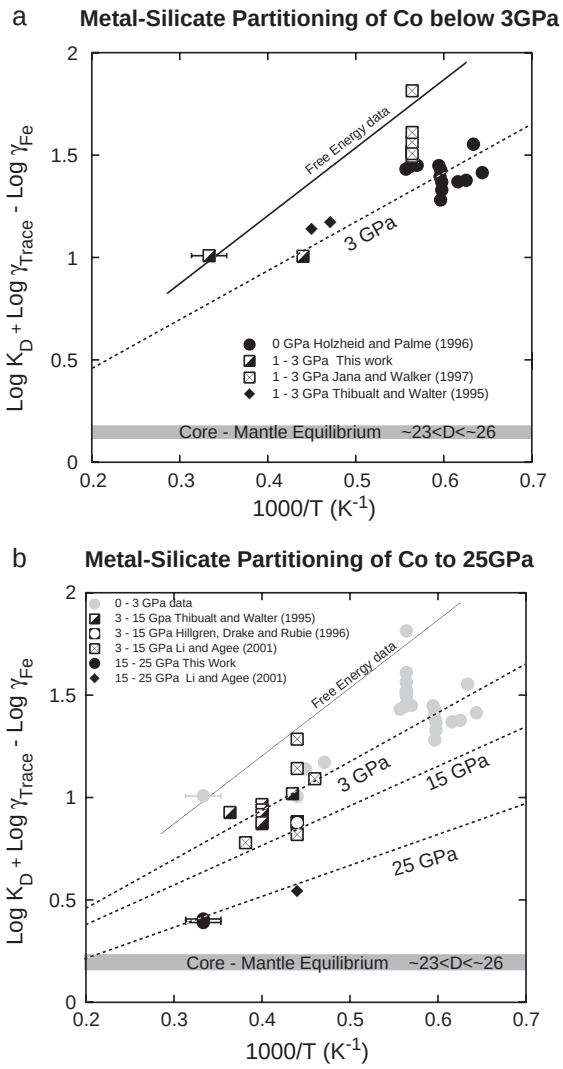

Fig. 4. Plot of Co partitioning data using the same approach as in Fig. 3. Solid lines represent 1 bar free energy data taken from [29,30], while dashed lines correspond to the best-fit equation at 3, 15 and 25 GPa (see text). The horizontal dark grey field represents the values of equilibrium constant required to generate the observed mantle abundance of Co ([5,7]). This corresponds to $D_{Co} = \frac{[Co]_{metal}}{[Co]_{silicate}}$ of about 23 to 26 (Table 2). Data taken from [14,46–50].

$VO_{1.5}$. Although highly charged ($\geq +4$) trace cations appear not to behave in a similar manner to FeO [28], the partitioning data for the major element Si show a trend parallel to the free energy data when we make the same assumption (Fig. 5a–b). Therefore we believe that the assumption of constant activity coefficient ratio in silicate melts is adequate for $(FeO)^2/SiO_2$. In order to constrain the temperature dependences of log K_a, we took 1 bar free energy

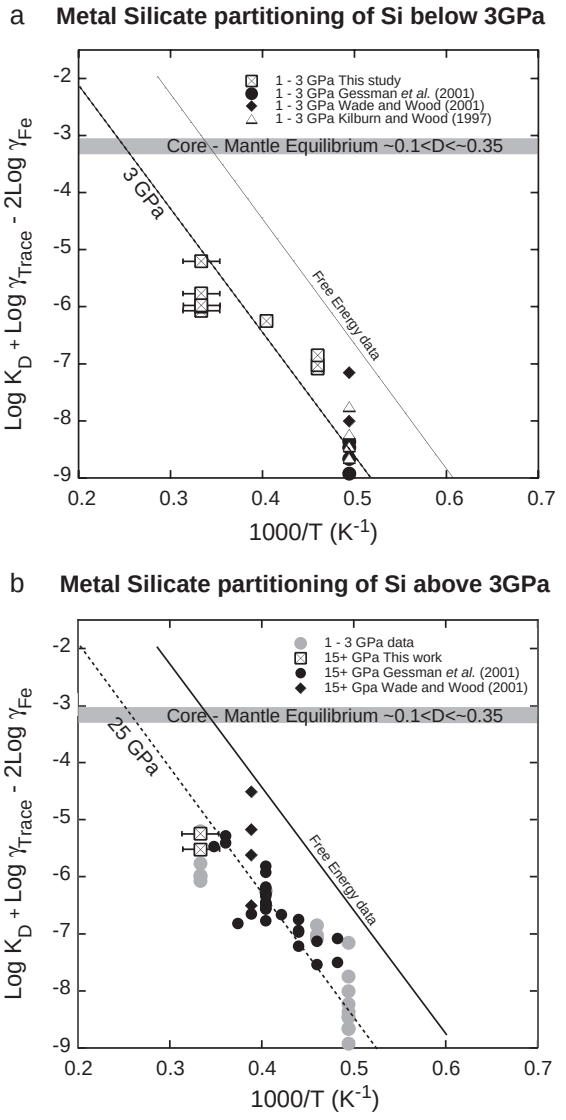

Fig. 5. Partitioning data for Si, $\log\left[K_D^{Si}\right] + \log\left(\gamma_{Si}^{met}\right) - \log\left(\gamma_{Fe}^{met}\right)^2$ plotted versus $1000/T$, in the same manner as Figs. 2–4. Solid lines represent 1 bar free energy data taken from [29,30], while dashed lines correspond to the best-fit equation at 3 and 25 GPa (see text). The horizontal dark grey field represents the values of equilibrium constant required to generate core concentrations of 2 to 7% Si ([5,7]). These correspond to $D_{Si} = \frac{[Si]_{metal}}{[Si]_{silicate}}$ of 0.1 to 0.35 (Table 2). Data taken from [46,51,52].

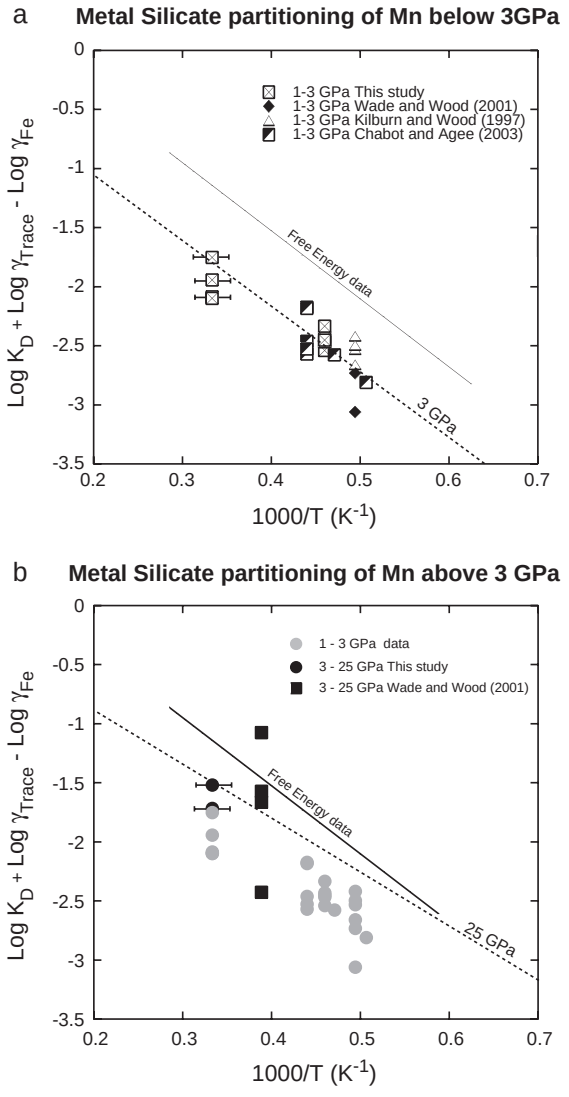

Fig. 6. Experimental partitioning data for Mn plotted in the same manner as Figs. 2–5. As before, solid lines represent 1 bar free energy data taken from [29,30], while dashed lines correspond to the best-fit equation at 3 and 25 GPa . Data taken from [31,46,52].

data from the literature [28–30] and plotted them on Figs. 2–6. As can be seen the free energy data parallel the trends of the partitioning results on the reciprocal temperature plots but are offset from them, partly because the activity coefficient ratio in the silicate is different from 1 and partly because of pressure effects on partitioning.

5. Results

Fig. 2 shows partitioning data for Vanadium plotted as a function of reciprocal temperature. As can be seen, the slope of the partitioning data is in excellent agreement with that obtained from free energy data [29,30]. A cursory examination suggests that the effect of pressure, based on the 25 GPa experiments, is very small. We fixed the temperature dependence at that given by the free energy data and regressed the partitioning data for the pressure term by assuming that the volume change of the exchange reaction (7) is constant, i.e to an equation of form:

$$\log[K_D] + \log\frac{\left(\gamma_{\mathrm{M}}^{\mathrm{met}}\right)}{\left(\gamma_{\mathrm{Fe}}^{\mathrm{met}}\right)^{n/2}} = A + \frac{B}{T} + \frac{cP}{T} \tag{8}$$

In Eq. (8), B is the temperature term which, in order to avoid errors in extrapolation, we have fixed at the value given by the thermodynamic tables [29,30] and P is the pressure in gigapascals. We then performed linear regression to obtain the intercept A and the pressure term c, with the following results:

$$\log\left[K_D^{\mathrm{V}}\right] + \log\frac{\left(\gamma_{\mathrm{V}}^{\mathrm{met}}\right)}{\left(\gamma_{\mathrm{Fe}}^{\mathrm{met}}\right)^{3/2}} = 0.34 - \frac{8548}{T} + \frac{24(\pm 23)P}{T}$$

Since the standard error in the regressed pressure term (± 23) is virtually the same as the value, 24, this term, as suggested by Chabot and Agee [31] is not significant. Applying the F-test leads to the same conclusion. Normally an F value of <0.05 would be required to add the pressure term to the equation and, in this case the F-value is 0.3. Therefore we excluded the pressure term and came to a final expression as follows:

$$\log\left[K_D^{\mathrm{V}}\right] + \log\frac{\left(\gamma_{\mathrm{V}}^{\mathrm{met}}\right)}{\left(\gamma_{\mathrm{Fe}}^{\mathrm{met}}\right)^{3/2}} = 0.27(\pm 0.07) - \frac{8548}{T}$$

For nickel the effects of both temperature and pressure are clear from the plot of partitioning data versus reciprocal temperature (Fig. 3). Constraining the temperature dependence of the equilibrium con-

stant using end-member free energy data leads to the following regressed equation:

$$\log\left[K_D^{\mathrm{Ni}}\right] + \log\frac{\left(\gamma_{\mathrm{Ni}}^{\mathrm{met}}\right)}{\left(\gamma_{\mathrm{Fe}}^{\mathrm{met}}\right)} = 0.64 + \frac{3097}{T} - \frac{123(\pm 9)P}{T}$$

In this case the pressure term is large (as one might expect from Fig. 3), easily passes the F-test and has a small standard error of 9.

The pressure effect on Co partitioning is generally acknowledged to be smaller than that for Ni [13,32]. Fig. 4 shows partitioning and free energy data at low and high pressures. If we regress the partitioning data and, as before, constrain the temperature effect with the free energy data we obtain:

$$\log\left[K_D^{\mathrm{Co}}\right] + \log\frac{\left(\gamma_{\mathrm{Co}}^{\mathrm{met}}\right)}{\left(\gamma_{\mathrm{Fe}}^{\mathrm{met}}\right)} = 0.01 + \frac{2511}{T} - \frac{45(\pm 11)P}{T}$$

It should be noted that, when modeling core formation, we found slightly better agreement between relative Ni and Co partitioning and the 'required' values of Table 2 if we adjusted the pressure terms by about 1 standard error to 114 for Ni and 55 for Co. These adjustments were made for the calculations described in the next section.

The depletion of Si, relative to other lithophile elements, in the silicate earth, may be due to sequestration in the core [5], or it may be due to a depletion of the bulk earth in Si due to slight volatility of the element [6]. At the moment we make no judgment except to say that if we assume sequestration in the core, then the required K_D values are given by the grey horizontal band in Fig. 5. Regressing the data and applying the constraint provided by the free energy data yields:

$$\log\left[K_D^{\mathrm{Si}}\right] + \log\frac{\left(\gamma_{\mathrm{Si}}^{\mathrm{met}}\right)}{\left(\gamma_{\mathrm{Fe}}^{\mathrm{met}}\right)^2} = 2.30 - \frac{21877}{T} + \frac{45(\pm 24)P}{T}$$

The pressure term is at the limit of normal tests of significance ($F=0.07$), but we retained it for our attempts to estimate the conditions of core formation. If we drop the pressure term the constant becomes 2.48 with a standard error of 0.07.

For manganese we make no assumption about the relative extents of depletion in the silicate earth due to initial volatility and dissolution in the core. The data of Fig. 6 yield the following result:

$$\log\left[K_D^{\mathrm{Mn}}\right] + \log\frac{\left(\gamma_{\mathrm{Mn}}^{\mathrm{met}}\right)}{\left(\gamma_{\mathrm{Fe}}^{\mathrm{met}}\right)} = 0.04 - \frac{5761}{T} - \frac{49(\pm 16)P}{T}$$

In addition to the data for these elements we have been allowed access to unpublished data of M.J. Walter (personal communication) on metal-silicate partitioning of W, Ga and P. Tungsten is of particular interest because it is a refractory element which is depleted in the silicate earth due to dissolution in the core. Using the best-fit oxidation state of +4, it is clear that, in this case, there is a strong dependence of K_D on the composition of the silicate melt. Having corrected for activity coefficients in the metal, we regressed the data as a function of pressure, temperature and silicate melt composition, in the latter case using the ratio of non-bridging oxygens to tetrahedral cations (NBO/Tet) as a proxy. This led to:

$$\log\left[K_D^{\mathrm{W}}\right] + \log\frac{\left(\gamma_{\mathrm{W}}^{\mathrm{met}}\right)}{\left(\gamma_{\mathrm{Fe}}^{\mathrm{met}}\right)^2} = 2.39 - \frac{1605}{T} - \frac{67.6P}{T} - 0.793\frac{\mathrm{NBO}}{\mathrm{Tet}}$$

For fertile peridotite, NBO/Tet is generally about 2.7. Phosphorus and gallium regressions performed by M.J. Walter and not corrected for other solutes were also used for comparison during our modeling

Table 2
Partition coefficients consistent with Core – Mantle equilibration

Element	McDonough and Sun 1995, McDonough 2003 [6,7]	Allegre et al. 1995 [5,7]	Likely range
D_P	22	45	20–50*
D_{Si}	0.29	0.34	0.1–0.35*
D_{V}	1.83	–	1.5–2.2
D_{Mn}	0.29	5	0.2–2.0*
D_{Fe}	13.66	13.65	13.65
D_{Co}	23.8	24.7	23–26
D_{Ni}	26.5	24.4	24–27
D_{Ga}	–	–	0–1.5*
D_{W}	16	–	15–22

* large uncertainty due to difficulty of constraining bulk Earth concentrations of volatile elements.

of core formation. These are, assuming peridotite liquid and an oxidation state of +5 for phosphorus:

$$\log\left[K_D^{\mathrm{P}}\right] = 0.64 - \frac{1593}{T} - \frac{74.95P}{T}$$

$$\log\left[K_D^{\mathrm{Ga}}\right] = -0.47 - \frac{114}{T} - \frac{215.5P}{T}$$

6. Application to Core Formation

The first important observation is that vanadium partition coefficients are, within uncertainty, dependent only on temperature. The implication is that we can extrapolate the temperature dependence (Fig. 2) until we reach the temperature necessary for core–mantle equilibration. The result is 3750 K at the current mantle Fe content of 6.26 wt.%. At this temperature and fixed mantle Fe content (or oxygen fugacity), the most pressure-sensitive element, Ni, requires a pressure of about 40 GPa for single-stage core–mantle equilibration. Under these conditions Ni, Co and W partitioning are all consistent with the values required to explain the current mantle concentrations of these elements (Table 1). The estimated Si content of the core is 10.5%, slightly above values based on cosmochemical data [5], while Ga and P partition coefficients are within the expected ranges of Table 1. Our estimated pressure and temperature conditions for single-stage equilibrium of 40 GPa at 3750 K are in good agreement with recent estimates based, in general on different experimental data sets. Gessmann and Rubie [33], for example, obtained values of 45 GPa at 3600 K from oxide-metal partitioning while Chabot and Agee [31] found temperatures of the order of 3600 K or higher to be appropriate.

Since accretion and core formation was a dynamic process, with the core probably beginning to separate when the planet was quite small [10] a single pressure and temperature of equilibration seems unreasonable. It is much more likely that the core separated over a wide range of pressures and temperatures as the planet grew. In order to simulate this process we assumed that, as the planet grew, the pressure corresponded to the base of the magma ocean. Constraining the temperature to have a mean of 3750 K and allowing pressure to increase as the planet grows, yields a possible P–T path consistent with V, Ni and Co partitioning given by the upper line on Fig. 7.

As can be seen from Fig. 7, the derived pressure–temperature conditions of equilibration, both for the single-stage process and for the dynamic process are, at constant oxygen fugacity (constant mantle Fe content) 700–1200 K above the peridotite liquidus ([34] [35]). This is physically implausible since the bottom of the magma ocean where the metal ponds (Fig. 1) must be at a temperature at which solid silicate is stable, i.e. at or below the liquidus. The implication is that the assumption of fixed oxygen fugacity requires the sinking droplets to cease equilibration during descent at a depth only half that of the magma ocean. This is physically implausible.

Our next step was to consider the conditions required both to fit the mantle abundances of the elements of interest and remain on the peridotite liquidus. We found that this can be readily achieved provided that the iron content of the mantle (oxygen fugacity) increases during accretion. Fig. 8 shows the results obtained if there is a step in oxygen fugacity from about 4 log units below the IW buffer (0.63% Fe in the mantle) to 2 log units below IW (6.26% Fe in the mantle) after 35% of accretion. For this calculation we accreted the earth in 1% steps and fixed the pressure at 46% of the value at the core mantle boundary i.e as the earth grew the magma ocean depth is fixed at about half the depth to the core–mantle boundary. As can be seen from Fig. 8, the bulk partition coefficients (D_i) of V, Ni, Co, W and P, despite varying greatly during accretion, are all in agreement with the expected ranges of Table 1. In this simplified dynamic accretion scenario the core contains 7% Si, in excellent agreement with cosmochemical estimates [5–7] and 1150 ppm Mn. Apart from Si, we made no explicit provision for the presence of 'light' elements in the metal since the core concentrations of such components are very uncertain ([5–7,36]) . When fixed on the peridotite liquidus, the mean temperature of accretion drops to 2990 K, which is within the experimental range. Thus, temperature extrapolations are minimized and we can have more confidence in the results. Since a discrete step is unlikely, we next assumed a gradual increase from 4 to 2 log units below IW over the interval 20–50% of accretion. As might be expected, results, shown in Fig. 9, are quite

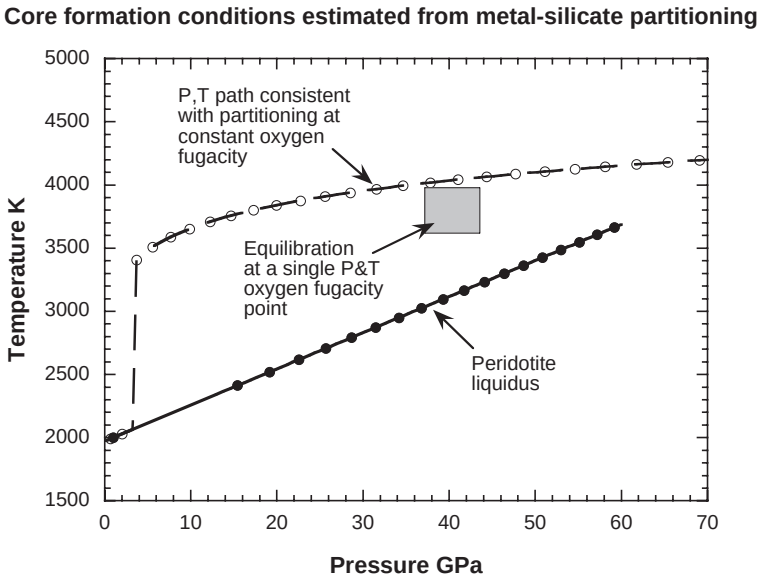

Fig. 7. Core formation conditions estimated using the metal-silicate partitioning data summarized in Figs. 2–6 with the requirement that partition coefficients for V, Ni, Co and W match the 'required' values in Table 1. For equilibrium to have occurred at an oxygen fugacity fixed by the current FeO content of the mantle, the temperatures required are in excess of the peridotite liquidus (taken from [34] [35]). This applies whether a single pressure, temperature equilibration point is assumed (shaded box) or a *P*,*T* path is followed (upper line). The implication is that, at fixed oxygen fugacity, descending metal droplets would have had to cease equilibrating with the silicate melt before they reached the bottom of the magma ocean defined by pressures and temperatures on the peridotite liquidus (see text).

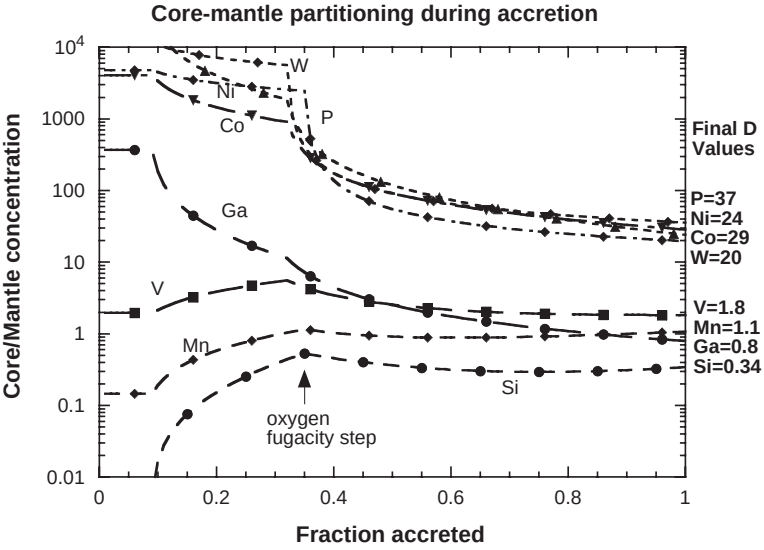

Fig. 8. Model of continuous core segregation during accretion. In this case the core segregates at the base of a magma ocean which is 46% of the depth to the core–mantle boundary. During accretion pressure increases with the mass of the Earth and the temperature path is fixed on the peridotite liquidus. There is an oxygen fugacity jump (from 4 log units to 2 log units below the iron–wüstite buffer corresponding to a jump from 0.63% to 6.36% Fe in the mantle), after 35% accretion. The mean temperature of accretion is 2990 K, and bulk partition coefficients are in agreement with (required) values of Table 2 (see text).

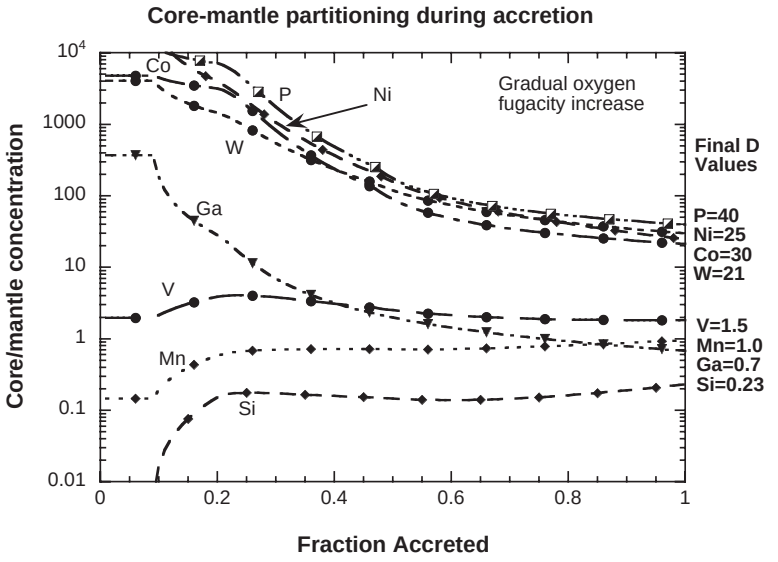

Fig. 9. Similar to Fig. 8 except the increase in oxygen fugacity is gradual, taking place over the interval of 20% to 50% accretion. As before, the required bulk partition coefficients are achieved for a *P–T* path along the peridotite liquidus with a mean temperature of 2990 K (see text).

similar to those with the oxygen fugacity step and yield the required partitioning behaviour for current mantle contents of V, Ni, Co, W and P. Since the accretion scenario is the same, the mean temperature remains 2990 K and, in this case, the core contains 5% Si.

In summary, single-step core formation scenarios, at fixed pressure, temperature and oxygen fugacity, can yield agreement with the observed mantle abundances of the refractory elements V, Ni, Co and W. The required temperature is, however, about 700 K above the peridotite liquidus, a result which is physically unrealistic for a magma ocean scenario. If we assume that, as the earth grew, the base of the deepening magma ocean remained on the peridotite liquidus, then the only possible solution requires the oxygen fugacity to have increased during accretion. In the simple scenario used here the magma ocean remained about half as deep as the mantle during accretion of the earth. This gives a pressure rising to 60 GPa. The observed mantle depletions in the refractory elements V, Ni, Co and W are reproduced provided that oxygen fugacity increases by about 2 log units during accretion. Given this constraint core equilibration remains on the liquidus and the metal contains between 5% and 7% Si, in good agreement with cosmochemical estimates.

The final question is, given that an increase in oxygen fugacity during accretion is required, how did this occur?

7. Oxidation of the Earth during Accretion

One possible explanation of our results is that the later stages of accretion involved impactors richer in FeO than the early stages [12,37], thus inducing an increase in the iron content of the mantle and concomitant increase in oxygen fugacity. Unfortunately, although perhaps correct, this is an untestable hypothesis. Another possibility is that oxidation arose due to dissociation of H_2O and escape of H_2 from the earth's atmosphere [38]. Although this mechanism must have operated to some extent, it is difficult to quantify. If it was the most important mechanism controlling the oxidation state of the earth's mantle then it is difficult to see why Mars, a more volatile-rich planet than Earth, with a higher FeO content [9] produces basalts which are more reduced than MORB [39]. As an alternative, we propose that the size of the Earth, in particular its ability to crystallize silicate perovskites through the pressure range of most of the mantle, is the factor controlling mantle oxidation state.

At depths below 660 km in the present-day Earth, the stable phases are magnesium silicate perovskite (79% by volume [40]), magnesiowüstite (16%) and calcium silicate perovskite 5%). An important property of magnesium silicate perovskite is that it accommodates the 5% Al_2O_3 which it dissolves in peridotite compositions by a coupled substitution with Fe^{3+} [41,42] as follows:

$$Mg^{2+}Si^{4+} \leftrightarrow Fe^{3+}Al^{3+}$$

It has recently been discovered that this substitution mechanism is so stable that it forces ferrous iron to disproportionate to ferric iron plus iron metal [43]:

$$3Fe^{2+} \leftrightarrow 2Fe^{3+} + Fe^{0} \quad (9)$$

Or, in terms of oxide components of the lower mantle:

$$3FeO + Al_2O_3 = \underset{\text{perovskite}}{2FeAlO_3} + \underset{\text{metal}}{Fe^0}$$

This means that, as perovskite began to crystallize from the magma ocean, it dissolved ferric iron as $FeAlO_3$ component and produced Fe metal. Since the perovskite is stable above 23 GPa, this process was taking place over a substantial part of the history of Earth's accretion and core formation. The implications are that metal sinking through the lower mantle to the core would inevitably have dissolved some of this internally-produced Fe, resulting in a perovskitic layer which was relatively oxidized. Given the gravitational instability of any metal layer (Fig. 1), accretional energies and heat-loss, it is inevitable that the depth of the magma ocean fluctuated continuously, thereby generating fronts of dissolution and precipitation at the lower boundary, as depicted in Fig. 10. This resulted in perovskite dissolution and re-precipitation acting as a ferric or oxygen 'pump', releasing ferric iron to the magma ocean during dissolution and producing more during precipitation. Thus the magma ocean became progressively oxidized. Later droplets of metal falling through the magma ocean would have reacted with the ferric iron driving reaction 9 to the left and producing more Fe^{2+} which then would dissolve in the silicate melt. Thus, the content of oxidized iron of the mantle (magma ocean) increased naturally as a consequence of perovskite crystallization, raising

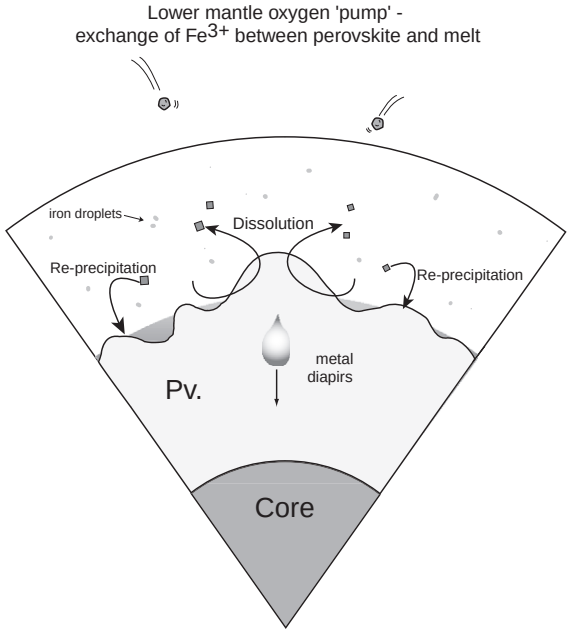

Fig. 10. Core formation accompanied by mantle 'self-oxidation' as a result of perovskite precipitation. Perovskite growth forces disproportionation of $Fe^{2+}$to Fe^{3+}(dissolved in perovskite) and Fe^0 (metal segregated to the core). The repeated crystallisation and dissolution of Fe^{3+}-containing perovskite acts as an oxygen 'pump', raising the oxygen fugacity of the growing mantle by releasing ferric iron to the magma ocean.

the oxygen fugacity of core segregation. In the very final stages of earth accretion this mechanism may have caused sufficient oxidation to halt metal segregation, thus setting the stage for the 'late veneer' to establish the mantle contents of highly siderophile elements [44].

The mantle self-oxidation mechanism discussed above has the advantage that it is based on a process which is experimentally observed to take place when magnesium silicate perovskite crystallizes [43]. It is therefore not necessary to make ad hoc assumptions about the compositions of the materials added to the Earth during accretion. The oxidation-state change required by partitioning data is a simple consequence of the size of the Earth. Any planet in which magnesium silicate perovskite is an important crystallizing phase must undergo the same process. The significance of perovskite to the oxidation state of the mantle perhaps explains why terrestrial basalts are more oxidized than those of Mars [39]. In the latter planet

perovskite should only be stabilized at pressures close to the core–mantle boundary. Therefore Mars did not undergo the same period of extensive perovskite crystallization during accretion as did the Earth.

8. Conclusions

The concentrations of the refractory elements V,Ni,Co and W in the earth's mantle constrain the conditions of core formation. If we assume single-stage core–mantle equilibrium at the oxygen fugacity defined by the current iron content of the mantle, then a pressure of 40 GPa at a temperature of 3750 K is obtained. Although these calculated conditions are in good agreement with others based on different datasets [31,33], they correspond to a temperature about 700 K above the peridotite liquidus. This is physically implausible since the base of the magma ocean, where metallic iron would pond, must be saturated in crystals and hence close to the mantle liquidus. Taking account of the accretion process and allowing multi-stage equilibrium as the earth accreted does not improve the discrepancy so long as the oxygen fugacity is constant.

In order to fix the temperature of the base of the magma ocean on the mantle liquidus and still match the observed mantle abundances of siderophile elements, we find that it is necessary for the fugacity of oxygen to increase during accretion. Simple models in which the base of the magma ocean remained at about half the depth of the mantle as the earth grew can match the observed abundances of V, Ni, Co and W provided the oxygen fugacity increased by about 2 log units. Either a step or gradual increase in Fe content of the mantle from about 0.63 to 6.26 wt.% during accretion produces the required result. Furthermore, the resultant average temperature of 2990 K is within the experimental range and hence more reliable than the high value of 3750 K obtained assuming single-stage core segregation. These models, or others involving an increase in oxidation state, generate a core containing 5 to 7 wt.% Si, a result in good agreement with cosmochemical estimates [5–7].

Although it has been suggested before that the earth grew heterogeneously, with more oxidized materials being added late in the accretion process, we argue here that the mantle self-oxidised. This occurred because the magnesium silicate perovskite which is the principal constituent of the lower mantle, forced the disproportionation of Fe^{2+} into Fe^{3+} plus metal [43]. During core segregation, this process, when coupled with dissolution and re-precipitation at the base of the magma ocean acted as an 'oxygen pump', raising the ferric iron content of the magma ocean. Later infalling metal was oxidized by the ferric iron, raising the FeO content of the silicate magma and the oxygen fugacity of core separation.

Acknowledgements

The authors would like to thank Mike Walter for permitting us to use unpublished experimental data, Dan Frost for his help with the multianvil experiments performed at Bayreuth and Stuart Kearns for analytical assistance. Experiments at Bayreuth were performed with assistance from the EU Large Scale Facility programme and additional support was provided by a Max Planck Research Award (to BJW).

References

[1] Q.Z. Yin, S.B. Jacobsen, K. Yamashita, J. Blichert-Toft, P. Telouk, F. Albarede, A short timescale for terrestrial planet formation from Hf–W chronometry of meteorites, Nature 418 (2002) 949–952.
[2] T. Kleine, C. Munker, K. Mezger, H. Palme, Rapid accretion and early core formation on asteroids and the terrestrial planets from Hf–W chronometry, Nature 418 (2002) 952–955.
[3] A.N. Halliday, Mixing, volatile loss and compositional change during impact-driven accretion of the Earth, Nature 427 (2004) 505–509.
[4] R.M. Canup, Origin of terrestrial planets and the Earth–Moon system, Physics Today 57 (2004) 56–62.
[5] C.J. Allegre, J.-P. Poirier, E. Humler, A.W. Hofmann, The chemical composition of the Earth, Earth and Planetary Science Letters 134 (1995) 515–526.
[6] W.F. McDonough, S.-s. Sun, The composition of the Earth, Chemical Geology 120 (1995) 223–253.
[7] W.F. McDonough, Compositional models for the Earth's core, in: R.W. Carlson (Ed.), The Mantle and Core, vol. 2, Elsevier-Pergamon, Oxford, 2003, pp. 547–568.
[8] H.E. Newsom, Accretion and Core Formation in the Earth: Evidence from Siderophile Elements, Oxford University Press, New York, 1990.
[9] H. Wanke, Constitution of the terrestrial planets, Philosophical Transactions of the Royal Society of London. A 303 (1981) 287–302.

[10] D.J. Stevenson, Models of the Earth's core, Science 214 (1981) 611–619.
[11] C.L. Chou, Fractionation of siderophile elements in the Earth's upper mantle, Ninth Lunar and Planetary Science Conference, 1978, pp. 219–230.
[12] H.S.C. O'Neill, The origin of the moon and the early history of the Earth — A chemical model, Geochimica et Cosmochimica Acta 55 (1991) 1159–1172.
[13] J. Li, C.B. Agee, Geochemistry of mantle–core differentiation at high pressure, Nature 381 (1996) 686–689.
[14] J. Li, C.B. Agee, The effect of pressure, temperature, oxygen fugacity and composition on partitioning of nickel and cobalt between liquid Fe–Ni–S alloy and liquid silicate: implications for the earth's core formation, Geochimica et Cosmochimica Acta 65 (2001) 1821–1832.
[15] K. Righter, M.J. Drake, Effect of water on metal-silicate partitioning of siderophile elements: a high pressure and temperature terrestrial magma ocean and core formation, Earth and Planetary Science Letters 171 (1999) 383–399.
[16] D.C. Rubie, H.J. Melosh, J.E. Reid, C. Liebske, K. Righter, Mechanisms of metal-silicate equilibration in the terrestrial magma ocean, Earth and Planetary Science Letters 205 (2003) 239–255.
[17] M.A. Bouhifd, A.P. Jephcoat, The effect of pressure on partitioning of Ni and Co between silicate and iron-rich metal liquids: a diamond-anvil cell study, Earth and Planetary Science Letters 209 (2003) 245–255.
[18] V.R. Murthy, Early differentiation of the earth and the problem of mantle siderophile elements — a new approach, Science 253 (1991) 303–306.
[19] D. Bouchard, C.W. Bale, Simultaneous-optimization of thermochemical data for liquid–iron alloys containing C, N, Ti, Si, Mn, S, and P, Metall. Mater. Trans., B, Proc. Metall. Mater. Proc. Sci. 26 (1995) 467–484.
[20] J. Wade, B.J. Wood, A high-temperature (3000 K) assembly for piston cylinder experiments, Geochemistry, Geophysics, and Geosystems 3 (2002) (art. no.-1006).
[21] D.J. Frost, B.T. Poe, R.G. Tronnes, C. Liebske, A. Duba, D.C. Rubie, A new large-volume multianvil system, Physics of the Earth and Planetary Interiors 143–44 (2004) 507–514.
[22] D.C. Rubie, Characterising the sample environment in multianvil high-pressure experiments, Phase Transitions 68 (1999) 431–451.
[23] J.S.f.t.P.o.S.a.T.t.C.o. Steelmaking, Steelmaking Data Sourcebook, Gordon and Breach Science Publishers, Montreux, 1988.
[24] C. Wagner, Thermodynamics of Alloys, Addison-Welsley, Reading, MA, 1962.
[25] C.W. Bale, A.D. Pelton, The unified interaction parameter formalism — thermodynamic consistency and applications, Metallurgical Transactions, A, Physical Metallurgy and Materials Science 21 (1990) 1997–2002.
[26] Z.T. Ma, Thermodynamic description for concentrated metallic solutions using interaction parameters, Metallurgical and Materials Transactions. B, Process Metallurgy and Materials Processing Science 32 (2001) 87–103.
[27] J.H. Jones, D.J. Malvin, A nonmetal interaction-model for the segregation of trace-metals during solidification of Fe–Ni–S, Fe–Ni–P, and Fe–Ni–S–P Alloys, Metallurgical Transactions. B, Process Metallurgy 21 (1990) 697–706.
[28] H.S.C. O'Neill, S.M. Eggins, The effect of melt composition on trace element partitioning: an experimental investigation of the activity coefficients of FeO, NiO, CoO, MoO2 and MoO3 in silicate melts, Chemical Geology 186 (2002) 151–181.
[29] I. Barin, F. Sauert, E. Schultze-Rhonhof, W.S. Sheng, Thermochemical Data of Pure Substances, Part I and Part II, CH Verlagsgesellschaft, Weinheim, Germany, 1989. 1739 pp.
[30] M.W. Chase, C.A. Davies, J.R. Downey, D.J. Frurip, R.A. McDonald, A.N. Syverud, Janaf thermochemical tables — 3rd Edition.1. Al-Co, Journal of Physical and Chemical Reference Data 14 (1985) 1–926.
[31] N.L. Chabot, C.B. Agee, Core formation in the Earth and Moon: new experimental constraints from V, Cr, and Mn, Geochimica et Cosmochimica Acta 67 (2003) 2077–2091.
[32] K. Righter, M.J. Drake, G. Yaxley, Prediction of siderophile element metal-silicate partition coefficients to 20 GPa and 2800 degrees C: the effects of pressure, temperature, oxygen fugacity, and silicate and metallic melt compositions, Physics of the Earth and Planetary Interiors 100 (1997) 115–134.
[33] C.K. Gessmann, D.C. Rubie, The origin of the depletions of V, Cr and Mn in the mantles of the Earth and Moon, Earth and Planetary Science Letters 184 (2000) 95–107.
[34] R.G. Tronnes, D.J. Frost, Peridotite melting and mineral-melt partitioning of major and minor elements at 22–24.5 GPa, Earth And Planetary Science Letters 197 (2002) 117–131.
[35] A. Zerr, A. Diegeler, R. Boehler, Solidus of Earth's deep mantle, Science 281 (1998) 243–246.
[36] D.C. Rubie, C.K. Gessmann, D.J. Frost, Partitioning of oxygen during core formation on the Earth and Mars, Nature 429 (2004) 58–61.
[37] H. Wanke, G. Dreibus, Chemical-composition and accretion history of terrestrial planets, Philosophical Transactions of the Royal Society of London, Series A: Mathematical and Physical Sciences 325 (1988) 545–557.
[38] D.M. Hunten, Atmospheric evolution of the terrestrial planets, Science 259 (1993) 915–920.
[39] C.D.K. Herd, L.E. Borg, J.H. Jones, J.J. Papike, Oxygen fugacity and geochemical variations in the martian basalts: implications for martian basalt petrogenesis and the oxidation state of the upper mantle of Mars, Geochimica et Cosmochimica Acta 66 (2002) 2025–2036.
[40] B.J. Wood, Phase transformations and partitioning relations in peridotite under lower mantle conditions, Earth and Planetary Science Letters 174 (2000) 341–354.
[41] C. McCammon, Perovskite as a possible sink for ferric iron in the lower mantle, Nature 387 (1997) 694–696.
[42] B.J. Wood, D.C. Rubie, The effect of alumina on phase transformations at the 660-kilometer discontinuity from Fe–Mg partitioning experiments, Science 273 (1996) 1522–1524.
[43] D.J. Frost, C. Liebske, F. Langenhorst, C.A. McCammon, R.G. Trønnes, D.C. Rubie, Experimental evidence for the

existence of iron-rich metal in the Earth's lower mantle, Nature 428 (2004) 409–412.
[44] H.S. O'Neill, The origin of the moon and the early history of the earth — a chemical-model. 2. The Earth, Geochimica et Cosmochimica Acta 55 (1991) 1159–1172.
[45] B.J. Wood, Carbon in the core, Earth and Planetary Science Letters 117 (1993) 593–607.
[46] J. Wade, B.J. Wood, The Earth's 'missing' niobium may be in the core, Nature 409 (2001) 75–78.
[47] V.J. Hillgren, M.J. Drake, D.C. Rubie, High pressure and high temperature metal-silicate partitioning of siderophile elements: the importance of silicate liquid composition, Geochimica et Cosmochimica Acta 60 (1996) 2257–2263.
[48] A. Holzheid, H. Palme, The influence of FeO on the solubilities of cobalt and nickel in silicate melts, Geochimica et Cosmochimica Acta 60 (1996) 1181–1193.
[49] D. Jana, D. Walker, The influence of sulfur on partitioning of siderophile elements, Geochimica et Cosmochimica Acta 61 (1997) 5255–5277.
[50] Y. Thibault, M.J. Walter, The influence of pressure and temperature on the metal-silicate partition-coefficients of nickel and cobalt in a model-C1 chondrite and implications for metal segregation in a deep magma ocean, Geochimica et Cosmochimica Acta 59 (1995) 991–1002.
[51] C.K. Gessmann, B.J. Wood, D.C. Rubie, M.R. Kilburn, Solubility of silicon in liquid metal at high pressure: implications for the composition of the Earth's core, Earth and Planetary Science Letters 184 (2001) 367–376.
[52] M.R. Kilburn, B.J. Wood, Metal-silicate partitioning and the incompatibility of S and Si during core formation, Earth and Planetary Science Letters 152 (1997) 139–148.